Acta Pharmaceutica Sinica B 2025;15(3):1535−1551

Chinese Pharmaceutical Association
Institute of Materia Medica, Chinese Academy of Medical Sciences

Acta Pharmaceutica Sinica B

www.elsevier.com/locate/apsb
www.sciencedirect.com

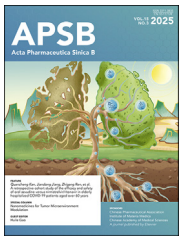

ORIGINAL ARTICLE

STK39 inhibits antiviral immune response by inhibiting DCAF1-mediated PP2A degradation

Chengfei Zhang[a,b,c,d,e,†,*], Ping Xu[c,†], Yongsheng Wang[d,†], Xin Chen[a,†], Yue Pan[a], Zhijie Ma[f], Cheng Wang[d], Haojun Xu[e], Guoren Zhou[g,*], Feng Zhu[a,*], Hongping Xia[b,c,d,e,*]

[a]*Department of General Surgery, Sir Run Run Hospital, Nanjing Medical University, Nanjing 211166, China*
[b]*Zhongda Hospital, School of Medicine, Advanced Institute for Life and Health, Southeast University, Nanjing 210009, China*
[c]*The Second Hospital Affiliated Wannan Medical College, Wuhu 241000, China*
[d]*Nanjing Drum Tower Hospital, The Affiliated Hospital of Nanjing University Medical School, Nanjing 210009, China*
[e]*National Health Commission Key Laboratory of Antibody Techniques & Department of Pathology, School of Basic Medical Sciences, Nanjing Medical University, Nanjing 211166, China*
[f]*Department of Pathology, Sir Run Run Shaw Hospital, School of Medicine, Zhejiang University, Hangzhou 310020, China*
[g]*Jiangsu Cancer Hospital, the Affiliated Cancer Hospital of Nanjing Medical University, Jiangsu Institute of Cancer Research, Nanjing 210009, China*

Received 13 January 2024; received in revised form 25 November 2024; accepted 27 December 2024

KEY WORDS

Viral infection;
Immune escape;
STK39;
PP2A;
PPP2R1A;
IRF3;
DCAF1;
Type I interferon

Abstract Evading host immunity killing is a critical step for virus survival. Inhibiting viral immune escape is crucial for the treatment of viral diseases. Serine/threonine kinase 39 (STK39) was reported to play an essential role in ion homeostasis. However, its potential role and mechanism in viral infection remain unknown. In this study, we found that viral infection promoted STK39 expression. Consequently, overexpressed STK39 inhibited the phosphorylation of interferon regulatory factor 3 (IRF3) and the production of type I interferon, which led to viral replication and immune escape. Genetic ablation or pharmacological inhibition of STK39 significantly protected mice from viral infection. Mechanistically, mass spectrometry and immunoprecipitation assays identified that STK39 interacted with PPP2R1A (a scaffold subunit of protein phosphatase 2A (PP2A)) in a kinase activity-dependent manner. This interaction

*Corresponding authors.
E-mail addresses: chengfeizhang@njmu.edu.cn (Chengfei Zhang), zhouguoren888@njmu.edu.cn (Guoren Zhou), zhufeng@njmu.edu.cn (Feng Zhu), 101013473@seu.edu.cn (Hongping Xia).
[†]These authors made equal contributions to this work.
Peer review under the responsibility of Chinese Pharmaceutical Association and Institute of Materia Medica, Chinese Academy of Medical Sciences.

https://doi.org/10.1016/j.apsb.2024.12.034

inhibited DDB1 and CUL4 associated factor 1 (DCAF1)-mediated PPP2R1A degradation, maintained the stabilization and phosphatase activity of PP2A, which, in turn, suppressed the phosphorylation of IRF3, decreased the production of type I interferon, and then strengthened viral replication. Thus, our study provides a novel theoretical basis for viral immune escape, and STK39 may be a potential therapeutic target for viral infectious diseases.

1. Introduction

Immune escape is a major obstacle to the treatment of viral diseases. As the first line of defense against virus infection, the innate immune system is an important barrier to virus immune escape. Interferons (IFN), in particular type I interferon, are critical antiviral cytokines in mammalian hosts, which establish the antiviral state by inducing transcription of interferon-stimulated genes (ISGs)[1-3]. Upon recognizing pathogen-associated molecular patterns (PAMPs), such as viral nucleic acids, host innate immune cells are activated by pathogen recognition receptors (PRRs), such as toll-like receptor (TLR), retinoic acid-inducible gene I (RIG-I)-like receptor (RLR) and cytoplasmic DNA receptors (CDRs). Interferon regulatory factor 3 (IRF3), a central transcription factor of type I interferon, is phosphorylated by the upstream kinases tank binding kinase 1 (TBK1), which then leads to the activation of IRF3, the expression of type I interferon and ISGs, and then eliminates the invading pathogens[4-8]. However, to successfully invade the host, viruses have developed numerous strategies to evade clearance by the innate immune system[9-11]. For example, the hepatitis C virus (HCV) NS4B protein abrogates RIG-I-mediated IFN-β production signaling by interacting with a stimulator of interferon genes (STING)[12]. Human cytomegalovirus (HCMV) glycoprotein US9 inhibits the expression of IFN-β by promoting MAVS leakage from the mitochondria and disrupting STING oligomerization and STING−TBK1 association[13]. Thus, exploring the mechanism of virus immune escape is critical for efficient viral clearance.

PP2A is a serine/threonine phosphatase and consists of a scaffolding A subunit, a regulatory B subunit, and a catalytic C subunit. More than half of the serine/threonine phosphatase activity in eukaryotic cells is carried out by PP2A. Thus, PP2A is important in modulating numerous signaling pathways in eukaryotes[14,15]. The activity of IRF3 is also controlled by PP2A. Previous studies indicate that the catalytic subunit of PP2A (PP2A-Cα) negatively regulates type I interferon signaling by dephosphorylating IRF3 and promotes viral infection[7], which reveals that the serine/threonine phosphatase activity of PP2A is essential for the regulation of IRF3-mediated type I interferon signaling. PPP2R1A is a well-recognized scaffold subunit of the PP2A complex and is critical for assembling the catalytic subunit and the regulatory B subunit. Mutation or deficiency of PPP2R1A may lead to decreased PP2A activity[16,17]. However, its role in the antiviral immune response is still unclear.

DCAF1, also named HIV-1 Vpr Binding Protein (VPRBP), is initially identified due to its interaction with HIV-1 Vpr protein[18,19]. Most studies indicate that DCAF1 is a putative substrate adaptor for the Cullin 4 A E3 ubiquitin ligase complex (CRL4−DCAF1 ubiquitin E3 ligase), which is ubiquitously expressed in different tissues and implicated in fundamental cellular processes, especially in regulating cell proliferation and DNA replication *via* binding to various substrates[20,21]. PP2A is a known substrate of CRL4−DCAF1 ubiquitin E3 ligase. CRL4−DCAF1 can bind to PPP2R1A and promote PPP2R1A poly-ubiquitination and proteasome degradation, which control the process of oocyte meiotic maturation[22]. This study demonstrates that DCAF1 can enhance antiviral immune response by facilitating PP2A degradation.

STK39 is a member of the STE20-like kinases family, also named SPAK. Full-length STK39 comprises a short N-terminal proline-alanine-rich domain (PAPA box), a kinase catalytic domain, and a C-terminal regulatory domain[23,24]. Previous studies reported that STK39 plays an important role in ion homeostasis by regulating the cation chloride cotransporters' activities, which is critical for the modulation of NaCl and blood pressure homeostasis[25,26]. The current studies identified that STK39 contributed to tumor progression[24,27]. Our studies also showed that STK39 promoted the progression of hepatocellular carcinoma by activating the PLK1/ERK signaling axis[28]. However, the role and the regulator mechanism of STK39 in viral infection remain obscure. Here, we report that viral infection dramatically upregulates STK39 expression. Overexpressed STK39 negatively regulates type I interferon signaling and facilitates viral replication by suppressing the phosphorylation of IRF3. Besides, inhibiting DCAF1-mediated PPP2R1A degradation contributes to suppressing the phosphorylation of IRF3. Taken together, our studies reveal that STK39 is crucial for viral immune escape and STK39 may be a potential therapeutic target for viral infectious diseases.

2. Materials and methods

2.1. Mice and viruses

Stk39$^{+/+}$ and *Stk39*$^{-/-}$ mice (in C57BL/6 background) were purchased from GemPharmatech (Nanjing, China). Mice were maintained in specific-pathogen-free facilities at the Animal Core Facility of Nanjing Medical University, and all animal experiments were approved by the Animal Care and Use Committee of Nanjing Medical University (Approval No. IACUC-2011019). VSV, VSV-GFP, NDV-GFP, and HSV-1 viruses were provided by Prof. Bing Du (East China Normal University)[29-31].

2.2. Antibodies and reagents

The antibodies used were as follows: anti-STK39 (Abcam and ABclonal), anti-phospho-IRF3 (Ser396) (Cell Signaling Technology), anti-phospho-TBK1 (Ser172) (Cell Signaling Technology), anti-phospho-JNK (Thr183/Tyr185) (Cell Signaling Technology), anti-phospho-AKT (Ser473) (Cell Signaling Technology), anti-

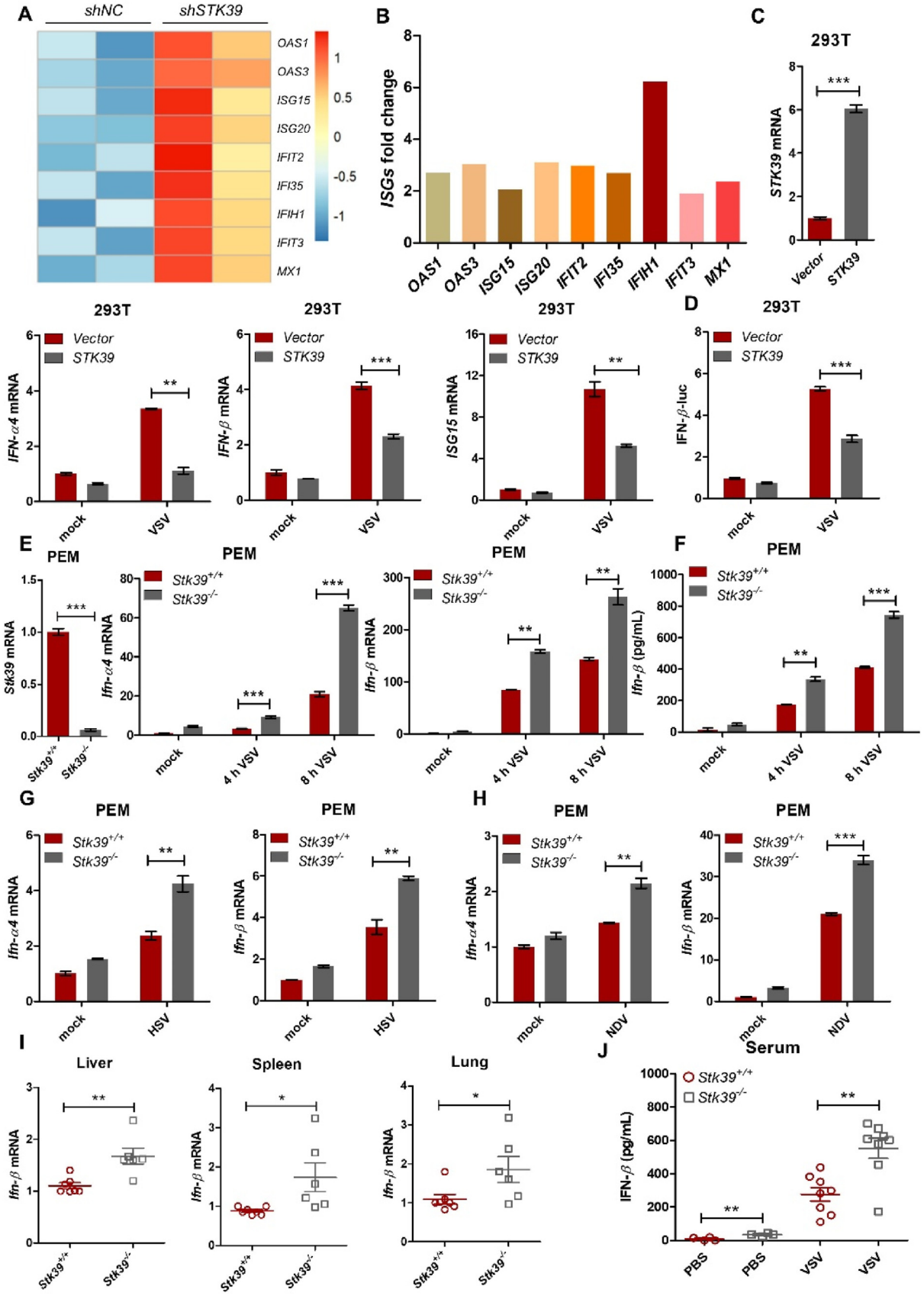

Figure 1 STK39 negatively regulates type I interferon signaling. (A, B) RNA-seq analyzes ISGs expression level after *STK39* knockdown in HuH7 cells. (C) Stable overexpression of STK39 in HEK293T cells, the cells were infected with VSV (MOI = 0.01) for 3 h. The expression of *STK39*, *IFN-α4*, *IFN-β*, and *ISG15* mRNA were analyzed by qPCR. (D) Overexpression of STK39 in HEK293T cells, the cells were co-

phospho-p65 (Ser536) (Cell Signaling Technology), anti-p65(Cell Signaling Technology), anti-AKT (Cell Signaling Technology), anti-IRF3 (Proteintech), anti-Flag (Proteintech), anti-HA (Proteintech), anti-PPP2R1A (Proteintech), anti-PPP2CA (Proteintech), anti-GST (Proteintech), anti-ubiquitin (Proteintech), anti-DCAF1 (Proteintech), anti-GAPDH (Proteintech), anti-TBK1 (ABclonal), anti-JNK (ABclonal), anti-K48-linkage specific Ubiquitin (ABclonal), goat anti-rabbit IgG(H + L) HRP secondary antibody (Bioworld), goat anti-mouse IgG(H + L) HRP secondary antibody (Bioworld), Zombie NIR™ Fixable Viability Kit (BioLegend), anti-mouse CD16/32 (BioLegend), APC anti-mouse CD45 (BioLegend), PerCP/Cyanine5.5 anti-mouse CD45 (BioLegend), FITC anti-mouse CD3 (BioLegend), PE anti-mouse CD8 (BioLegend), PerCP/Cyanine5.5 anti-mouse CD4 (BioLegend), APC anti-mouse CD11c (BioLegend), PE anti-mouse I-A/I-E (MHC class II) (BioLegend), APC anti-mouse F4/80 (BioLegend), FITC anti-mouse/human CD11b (BioLegend). STK39 inhibitors closantel and rafoxanide, SP600125, PDTC ammonium, mithramycin A, stattic, fludarabine, cycloheximide (CHX), MG-132, and 3-methyladenine (3-MA) were obtained from MedChemExpress.

2.3. Cell culture

RAW264.7 and HEK293T cells were obtained from the American Type Culture Collection. Bone marrow-derived macrophages (BMDMs) and peritoneal macrophages (PEMs) were prepared as described previously[32]. Cells were cultured in DMEM containing 10% FBS and 1% penicillin/streptomycin.

2.4. Virus infection

For cell infection, cells were seeded into 12-well plates overnight. The cells were pretreated with indicated concentrations of STK39 inhibitors for 1 h and then infected with VSV (MOI = 0.01), HSV-1 (MOI = 0.01), and NDV (MOI = 0.01 or 0.1) for 12 or 24 h, the supernatants from VSV-infected cells were collected for viral plaque assay, virus RNA replicates were detected by quantitative real-time PCR. For mice infection, age- and sex-matched groups of mice were intraperitoneally treated with STK39 inhibitor rafoxanide (5 mg/kg) for 3 h and then intraperitoneally infected with VSV (5×10^8 pfu/g) for 24 h, lung injury was examined by H&E staining assay and VSV RNA replicates in the organs were detected by quantitative real-time PCR.

2.5. CCK8 assay

RAW264.7 (5×10^4 cells per well) and HEK293T (2×10^4 cells per well) cells were seeded into 96-well plates overnight. The cells were then treated with indicated concentrations of STK39 inhibitors for 12 h, 10 μL CCK8 was added to each well and incubated at 37 °C for 1 h. After incubation, the absorbance value was measured at 450 nm.

2.6. Quantitative real-time PCR

Cells were lysed in total RNA Rapid Extraction Reagent (Yfxbio) and cDNA was synthesized from extracted total RNA using 5 × All-In-One RT MasterMix (ABMgood) according to the manufacturer's protocol. Quantitative Real-Time PCR (qPCR) was performed with SYBR Green Master Mix (YEASEN) and 500 ng cDNA was used as a template. GAPDH was used as an internal control gene. The sequence-specific primers are listed in Supporting Information Table S1.

2.7. Immunoblot analysis

Cells were lysed using RIPA buffer (50 mmol/L Tris, pH 7.4, 150 mmol/L NaCl, 2 mmol/L EDTA, 0.5% Nonidet P-40) supplemented with protease and phosphatase inhibitors. The concentrations of the extracts were measured using a BCA Protein Assay Kit (Thermo). The protein samples were separated by 10% SDS-PAGE, transferred onto nitrocellulose membranes and blocked with 5% BSA. The membranes were then incubated with appropriate primary and secondary antibodies. Protein bands were visualized using the chemiluminescence imaging system (Beijing Sage Creation).

2.8. Immunofluorescence

HEK293T cells were infected with VSV (0.001 or 0.01 MOI) for 12 h. Then, the cells were fixed with 4% paraformaldehyde in PBS for 30 min and permeabilized using 0.3% Triton X-100. After blocking with 5% BSA in PBS, cells were incubated with an anti-STK39 antibody overnight and stained with Cy3 goat anti-rabbit IgG(H + L) antibody (ABclonal). After staining nuclei with DAPI, the cells were visualized using a fluorescence microscope.

2.9. Viral plaque assay

For viral plaque assay, 2×10^5 Vero cells were seeded into 12-well plates overnight. The supernatants from VSV-infected cells were serially diluted and then treated the Vero cells for 1 h, the supernatant was removed and the Vero cells were covered with DMEM containing 1% low-melting-point agarose. After 24 h, plaques were counted.

2.10. ELISA assay

Supernatants from infected cells and serum from infected mice were collected. Levels of mouse IFN-β in cell supernatants and serum were detected by ELISA according to the manufacturer's instructions (BioLegend).

transfected with IFN-β promoter and *Renilla* reporter plasmids for 24 h and then infected with VSV (MOI = 0.01) for 3 h. IFN-β luciferase activities were measured with a dual-luciferase reporter assay system. (E, F) *Stk39*$^{+/+}$ and *Stk39*$^{-/-}$ PEMs were infected with VSV (MOI = 0.01) for the indicated times. The expression of *Stk39*, *Ifn-α4*, and *Ifn-β* were analyzed by qPCR and the production of IFN-β was measured by ELISA. (G, H) *Stk39*$^{+/+}$ and *Stk39*$^{-/-}$ PEMs were infected with HSV-1 or NDV for 12 h. The expression of *Ifn-α4* and *Ifn-β* were analyzed by qPCR. (I, J) Six-week-old *Stk39*$^{+/+}$ and *Stk39*$^{-/-}$ mice were intraperitoneally injected with VSV (5×10^8 pfu/g) for 12 h. The expression of *Ifn-β* in organs ($n = 7$/*Stk39*$^{+/+}$ group, $n = 6$/*Stk39*$^{-/-}$ group) was analyzed by qPCR and the production of IFN-β in serum ($n = 4$/*Stk39*$^{+/+}$ PBS group, $n = 4$/*Stk39*$^{-/-}$ PBS group, $n = 8$/*Stk39*$^{+/+}$ VSV group, $n = 8$/*Stk39*$^{-/-}$ VSV group) was measured by ELISA. Data are shown as mean ± SEM; $^*P < 0.05$; $^{**}P < 0.01$; $^{***}P < 0.001$.

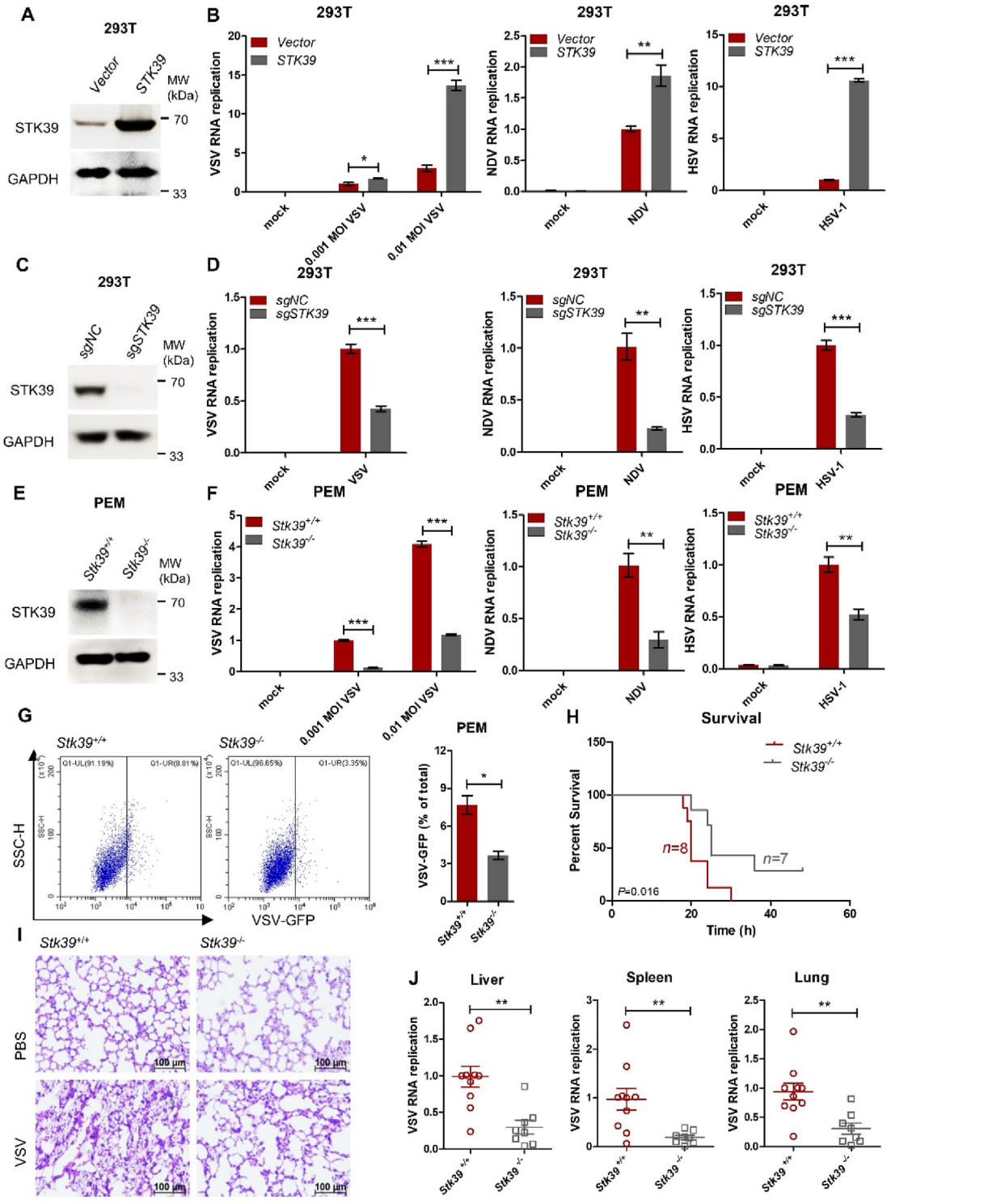

Figure 2 STK39 promotes viral infection. (A) HEK293T cells were transfected with an empty vector or STK39-overexpression plasmid for 48 h. The expression of STK39 was assessed by immunoblotting. (B) HEK293T cells were transfected with STK39-overexpression plasmid for 48 h and then infected with the indicated virus. Viral RNA replicates were detected by qPCR. (C) Immunoblotting identified that STK39 was knocked out in HEK293T cells using the CRISPR/Cas9 system. (D) Wild-type and *STK39*-knockout HEK293T cells were infected with the indicated virus. Viral RNA replicates were detected by qPCR. (E) Immunoblotting identified that Stk39 was knocked out in mouse PEMs. (F) $Stk39^{+/+}$ and $Stk39^{-/-}$ mice PEMs were infected with the indicated virus. Viral RNA replicates were detected by qPCR. (G) $Stk39^{+/+}$ and $Stk39^{-/-}$ mice PEMs were infected with VSV-GFP for 24 h, and GFP^{+} cells were analyzed by FACS. (H) $Stk39^{+/+}$ and $Stk39^{-/-}$ mice were infected with VSV (1×10^9 pfu/g) intraperitoneally, and the survival of mice was recorded for 48 h. (I, J) $Stk39^{+/+}$ and $Stk39^{-/-}$ mice were infected with VSV (5×10^8 pfu/g) intraperitoneally for 24 h, lung injury was examined by H&E staining assay (Scale bar, 100 μm) and VSV RNA replicates in the organs ($n = 10/Stk39^{+/+}$ group, $n = 8/Stk39^{-/-}$ group) were detected by qPCR. Data are shown as mean ± SEM; $^{*}P < 0.05$; $^{**}P < 0.01$; $^{***}P < 0.001$.

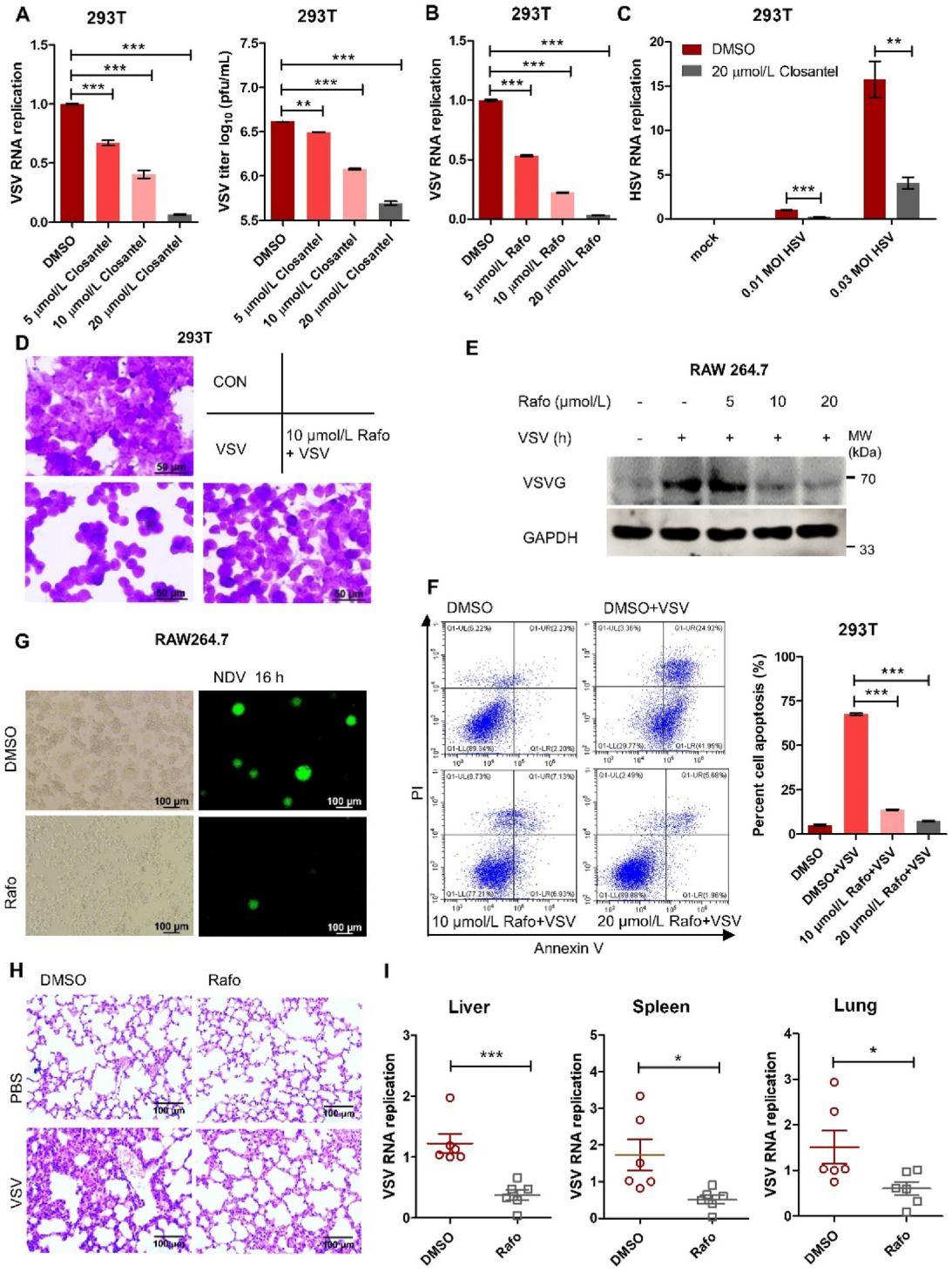

Figure 3 STK39 inhibitors protect cells and mice against viral infection. (A) HEK293T cells were pretreated with indicated concentrations of STK39 inhibitor closantel for 1 h and then infected with VSV (MOI = 0.01) for 12 h. VSV RNA replicates were detected by qPCR and VSV TCID50 of the supernatants were measured by viral plaque assay. (B) HEK293T cells were pretreated with indicated concentrations of STK39 inhibitor rafoxanide for 1 h and then infected with VSV (MOI = 0.01) for 12 h. VSV RNA replicates were detected by qPCR. (C) HEK293T cells were pretreated with 20 μmol/L closantel for 1 h and then infected with indicated MOI HSV-1 for 24 h. HSV-1 RNA replicates were detected by qPCR. (D) HEK293T cells were pretreated with 10 μmol/L STK39 inhibitor rafoxanide for 1 h and then infected with VSV (MOI = 0.01) for 12 h. The cells were stained with crystal violet and observed under a microscope. Scale bar, 50 μm. (E) RAW264.7 cells were pretreated with indicated concentrations of rafoxanide for 1 h and then infected with VSV (MOI = 0.01) for 12 h. The VSV-G protein expression levels were detected by immunoblotting. (F) HEK293T cells were pretreated with indicated concentrations of STK39 inhibitor rafoxanide for 1 h and then infected with VSV (MOI = 0.01) for 12 h. Apoptotic cells were detected by flow cytometry. (G) RAW264.7 cells were pretreated with 20 μmol/L rafoxanide for 1 h and then infected with NDV (MOI = 0.01) for 16 h. The cells were observed under a fluorescence microscope. Scale bars,

2.11. Immunoprecipitation

HEK293T cells were lysed using cell lysis buffer (50 mmol/L Tris, pH 7.4, 150 mmol/L NaCl, 2 mmol/L EDTA, 0.5% Nonidet P-40, 10% glycerol, EDTA-free protease inhibitor cocktail). Whole-cell extracts were clarified by protein G agarose and incubated with the appropriate antibodies plus protein G beads. The proteins were eluted with 2 × SDS loading buffer and assessed by immunoblotting.

2.12. GST pull-down assay

The fusion protein of GST-STK39 and GST protein were purified with Glutathione Sepharose beads (TransGen Biotech) from competent cells. The beads were washed three times and then incubated with His-PPP2R1A protein lysates at 4 °C for 4 h. Precipitates were washed three times, eluted with 2 × SDS loading buffer, and assessed by immunoblotting.

2.13. Construction of stable cell line

To generate stable overexpression, knockdown or knockout HEK293T cell lines, HEK293T cells were infected with lentivirus containing pLenti-CMV-STK39 (Biogot Technology), sgSTK39 (target sequence 5′-CAGGGACGCGTACGAGCTGC-3′) or DCAF1-shRNA plasmid (target sequence1: 5′-CGAGAAACTGAGTCAAATGAA-3′, target sequence2: 5′-GCGACTCATTCTCCAATATTT-3′) for 3 days and then screened with 2 μg/mL of puromycin about 1 week before being used in experiments.

2.14. Luciferase reporter assay

Control and STK39-overexpression HEK293T cells were plated into 12-well plates (3×10^5 cells per well) overnight and co-transfected with IFN-β reporter plasmid, *Renilla* plasmid and indicated overexpression plasmid for 24 h. Luciferase activity was measured with a Dual-Luciferase Assay System (Promega) and the activity of the reporter gene was normalized by *Renilla* luciferase activity.

2.15. Crystal violet staining assay

HEK293T cells were seeded into 12-well plates (3×10^5 cells per well) overnight. The cells were treated with STK39 inhibitor for 2 h and then infected with VSV (MOI = 0.01) for 12 h. The medium was removed, and the cells were then fixed with 4% paraformaldehyde in PBS for 30 min and stained with 0.1% crystal violet for 30 min at room temperature. The cells were washed with PBS three times and the photographs were taken under a bright-field microscope.

2.16. H&E staining assay

Lung tissues from viral-infected mice were dissected and fixed with 4% paraformaldehyde in PBS overnight. Tissues were then embedded into paraffin and cut into slices. After stained with hematoxylin/eosin solution (H&E), histological changes were examined by light microscopy.

2.17. Apoptosis assay

HEK293T cells were seeded into 6-well plates (6×10^5 cells per well) overnight. After being treated with STK39 inhibitor for 2 h, the cells were then infected with VSV (MOI = 0.1) for 12 h. The cells were stained with fluorescein isothiocyanate (FITC) Annexin V and propidium iodide (PI) and then detected by flow cytometry (CytoFLEX). Data were analyzed with CytExpert software.

2.18. Immune cell detection by flow cytometry

The spleen of mice was ground in FACS buffer (PBS supplemented with 2% FBS) and passed through a 70 μm cell strainer and followed red blood cell lysis. The cells were blocked FcγII/III with anti-CD16/32 at 4 °C for 20 min, and then stained with Zombie NIR™ Fixable Viability Kit (distinguish between live and dead cells) and specific antibodies at 4 °C for 30 min in the dark. The stained cells were analyzed by flow cytometry (CytoFLEX). Data were analyzed with CytExpert software.

2.19. Statistical analysis

All statistical analyses were performed by Student's *t*-test (two-tailed) using the GraphPad Prism software and a *P*-value <0.05 was considered statistically significant. All data were presented as mean ± standard error of mean (SEM).

3. Results

3.1. STK39 negatively regulates type I interferon signaling

To inspect the signaling pathways of STK39 regulated in organisms, the transcriptomic analysis was performed previously to identify gene expression changes in *STK39*-knockdown cells[28]. We found that numerous genes involved in the type I interferon signaling pathway (interferon-induced genes, ISGs) were significantly upregulated in *STK39*-knockdown cells (Fig. 1A and B). Considering the critical role of type I interferon signaling in antiviral innate immunity, we speculated that STK39 may play an important role in viral infection. To verify this speculation, we first assessed the influence of STK39 on type I interferon signaling. As shown in Fig. 1C, overexpression of STK39 in HEK293T cells significantly inhibits the expression of viral-induced *IFN-α4*, *IFN-β* and *ISG15*. A similar phenomenon was found in *Stk39*-overexpression RAW264.7 cells, and the monitoring of viral replication in cells revealed that the experimental conditions we selected were enough for the virus to successfully infect the host cells (Supporting Information Fig. S1A−S1C). Luciferase reporter assay also showed that transiently transfected HEK293T cells with *STK39*-expression plasmid decreased the activity of IFN-β luciferase (Fig. 1D). These results reveal that STK39 negatively regulates type I interferon signaling. To confirm that, *Stk39*-deficient mice ($Stk39^{-/-}$) were purchased from GemPharmatech (Nanjing, China). We infected $Stk39^{+/+}$ and $Stk39^{-/-}$ peritoneal macrophages

100 μm. (H, I) Wild-type mice were treated with 5 mg/kg STK39 inhibitor rafoxanide for 3 h and then infected with VSV for 24 h. Lung injury was examined by H&E staining assay (Scale bars, 100 μm) and VSV RNA replicates in the organs ($n = 6$/DMSO group, $n = 6$/Rafo group) were detected by qPCR. Data are shown as mean ± SEM; $^*P < 0.05$; $^{**}P < 0.01$; $^{***}P < 0.001$.

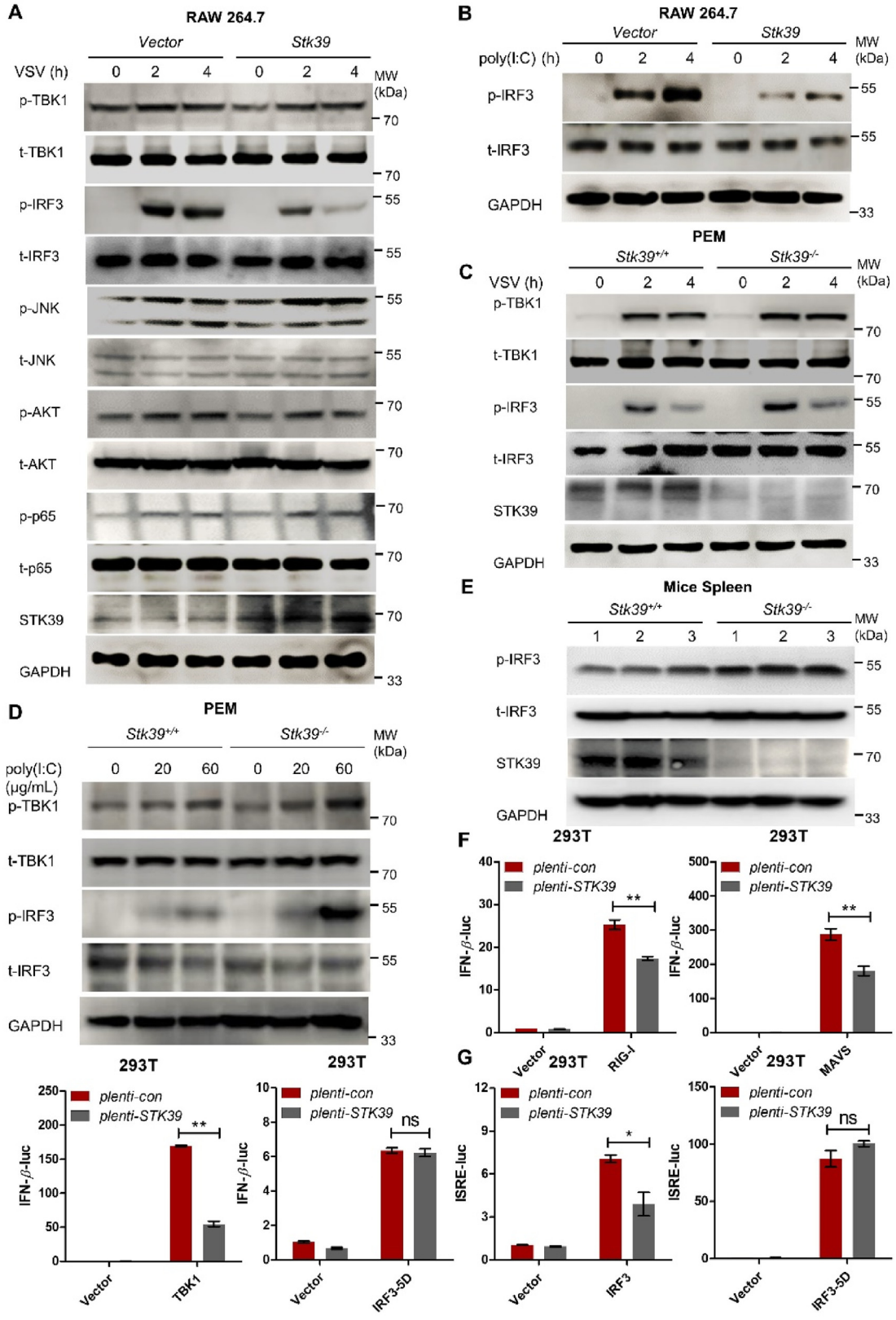

Figure 4 STK39 suppresses the phosphorylation of IRF3. (A) Stable overexpression of Stk39 in RAW264.7 cells, the cells were infected with VSV (MOI = 0.1) for the indicated times. The proteins involved in regulating IFN expression were assessed by immunoblotting. (B) Stable overexpression of Stk39 in RAW264.7 cells. The cells were transfected with 30 μg/mL poly(I:C) for the indicated times. Phosphorylated or total IRF3 were assessed by immunoblotting. (C) $Stk39^{+/+}$ and $Stk39^{-/-}$ PEMs were infected with VSV (MOI = 0.1) for the indicated times. Phosphorylated or total TBK1 and IRF3 were assessed by immunoblotting. (D) $Stk39^{+/+}$ and $Stk39^{-/-}$ PEMs were transfected with indicated

(PEMs) with VSV (RNA virus), NDV (RNA virus), or HSV-1 (DNA virus) and detected the expression of type I interferon. We found that the expression and production of type I interferon were significantly higher in *Stk39*$^{-/-}$ PEMs than in *Stk39*$^{+/+}$PEMs (Fig. 1E−H and Fig. S1D−S1F). In addition, *Stk39*-deficient mice expressed more *Ifn-β* in various organs and serum during viral infection (Fig. 1I, J and Fig. S1G). Consistent with these, we found that STK39 inhibitors significantly promoted the expression of *Ifn-β* in RAW264.7 macrophages (Fig. S1H). Thus, our results demonstrate that STK39 negatively regulates type I interferon signaling in antiviral innate immunity response.

To investigate the potential role of STK39 during viral infection, we then explored the correlation between STK39 expression level and viral infection. HEK293T cells and RAW264.7 cells were infected with VSV, NDV, HSV-1 or stimulated with viral RNA mimic poly(I:C). We found that the mRNA and protein levels of STK39 were significantly upregulated during viral infection or poly(I:C) stimulation (Fig. S1I and S1J and Supporting Information Fig. S2A−S2D). Immunofluorescence also showed that viral infection upregulated STK39 expression (Fig. S2E). These data suggest that STK39 expression was upregulated during viral infection. To further determine the mechanism underlying STK39 upregulation during viral infection, HEK293T cells were pretreated with multiple signaling pathway inhibitors before viral infection. As shown in Fig. S2F, NF-κB, SP1, and STAT1 inhibitors dramatically decreased viral infection-induced expression of STK39. This suggests that viral infection upregulates STK39 through multiple signaling pathways. Taken together, these data suggest that viral infection-induced STK39 expression negatively regulates type I interferon signaling. This reveals that STK39 may play an important role in viral immune escape.

Type I interferon signaling is also critical for the development of immune cells and is associated with autoimmune diseases. According to Fig. 1E−J results, knockout of *Stk39* tended to promote type I interferon expression in uninfected cells or mice. To evaluate whether knockout of *Stk39* leads to dysregulation of immune cells in mice, the distribution of immune cells in *Stk39*$^{+/+}$ and *Stk39*$^{-/-}$ mice spleens were analyzed by flow cytometry. The results show that knockout of *Stk39* had little impact on the immune cells (dendritic cells, macrophages, and T cells) development in spleens (Fig. S2G and S2H). Which excluded the possibility that knockout of *Stk39* caused autoimmune diseases in normal mice.

3.2. *STK39 facilitates viral infection*

To assess the biological significance of STK39 in viral infection, we transiently expressed STK39 in HEK293T cells and then challenged the cells with VSV, NDV, and HSV-1 for the indicated time. By measuring the viruses RNA level in the cells and the 50% tissue culture infective dose (TCID50) of the supernatant from the infected HEK293T cells, we found that overexpression of STK39 significantly promoted viral replication (Fig. 2A and B, Supporting Information Fig. S3A and S3B). Meanwhile, stable *Stk39*-overexpression RAW264.7 macrophages were constructed, and it was also found that overexpression of Stk39 in RAW264.7 macrophages promoted VSV replication (Fig. S3C). Consistent with this, knockout or knockdown of *STK39* in HEK293T cells suppressed viral replication (Fig. 2C and D, Fig. S3D). To further confirm the role of STK39 in viral infection, we used peritoneal macrophages (PEMs) from *Stk39*$^{+/+}$ (wild-type) and *Stk39*$^{-/-}$ mice to assess the effects of *Stk39* deficiency on viral infection. We found that knockout of *Stk39* in PEMs dramatically suppressed viral replication (Fig. 2E−G and Fig. S3E). A similar result was found in bone marrow-derived macrophages (BMDMs) (Fig. S3F). To further confirm this function of Stk39 *in vivo*, we challenged *Stk39*$^{+/+}$ and *Stk39*$^{-/-}$ mice with a lethal dose of VSV. As shown in Fig. 2H, *Stk39*$^{+/+}$ mice were more susceptible to VSV infection and had a higher mortality rate compared with *Stk39*$^{-/-}$ mice. Besides, VSV-induced lung injury was ameliorated in *Stk39*-deficient mice, and VSV replication in various organs (liver, spleen, and lung) was also decreased in *Stk39*-deficient mice (Fig. 2I and J). Taken together, these data suggest that *Stk39* deficiency protects mice from viral infection. STK39 has a negative role in regulating host defense against viruses.

3.3. *STK39 inhibitors ameliorate viral infection*

To evaluate the potential function of targeting STK39 in the treatment of viral diseases, STK39 inhibitors (closantel and rafoxanide) were selected to treat cell lines[33]. By testing VSV RNA level, VSV-GFP expression, and TCID50 of the supernatant from the infected HEK293T cells, we found that STK39 inhibitors closantel and rafoxanide markedly suppressed the VSV replication (Fig. 3A and B, Supporting Information Fig. S4A). The replication of DNA virus HSV-1 was also inhibited by closantel (Fig. 3C). By crystal violet staining assay, we found that STK39 inhibitor rafoxanide significantly ameliorated the VSV-induced cytopathic effect of HEK293T cells (Fig. 3D). Besides, the protein expression of vesicular stomatitis virus glycoprotein (VSV-G) in VSV-infected RAW264.7 cells was significantly decreased by STK39 inhibitor rafoxanide in a concentration-dependent manner (Fig. 3E). Moreover, VSV-induced cell death or apoptosis was also reduced by STK39 inhibitor rafoxanide (Fig. 3F). In addition to VSV and HSV-1 infection, the NDV-GFP virus was also used to infect RAW264.7 cells. As shown in Fig. 3G, Fig. S4B and S4C, GFP^{+} RAW264.7 cells and NDV RNA replication were all reduced in STK39 inhibitor-treated cells. To further confirm this function *in vivo*, mice were pretreated with STK39 inhibitor rafoxanide before being infected with VSV. As shown in Fig. 3H and I, we found that rafoxanide markedly ameliorated VSV-induced lung injury and VSV replication in various organs (liver, spleen, and lung). The cytotoxicity results showed that the function of STK39 inhibitors was not due to toxicity (Fig. S4D and S4E). Thus, these data suggest that STK39 inhibitors have broad-spectrum antiviral activities, which have great potential in protecting hosts from viral infection.

concentrations of poly(I:C) for 6 h. Phosphorylated or total TBK1 and IRF3 were assessed by immunoblotting. (E) Six-week-old *Stk39*$^{+/+}$ and *Stk39*$^{-/-}$ mice were intraperitoneally injected with VSV (5×10^8 pfu/g) for 12 h. Phosphorylated or total IRF3 in mice spleens was assessed by immunoblotting. (F) Stable overexpression of STK39 in HEK293T cells, the cells were co-transfected with IFN-β promoter reporter plasmid, renilla reporter plasmid, and the indicated protein plasmid for 24 h. The activities of IFN-β luciferase were measured with a dual-luciferase reporter assay system. (G) Stable overexpression of STK39 in HEK293T cells, the cells were co-transfected with ISRE promoter reporter plasmid, renilla reporter plasmid, and the indicated protein plasmid for 24 h. The activities of ISRE luciferase were measured with a dual-luciferase reporter assay system. Data are shown as mean ± SEM; *$P < 0.05$; **$P < 0.01$; ns, not significant.

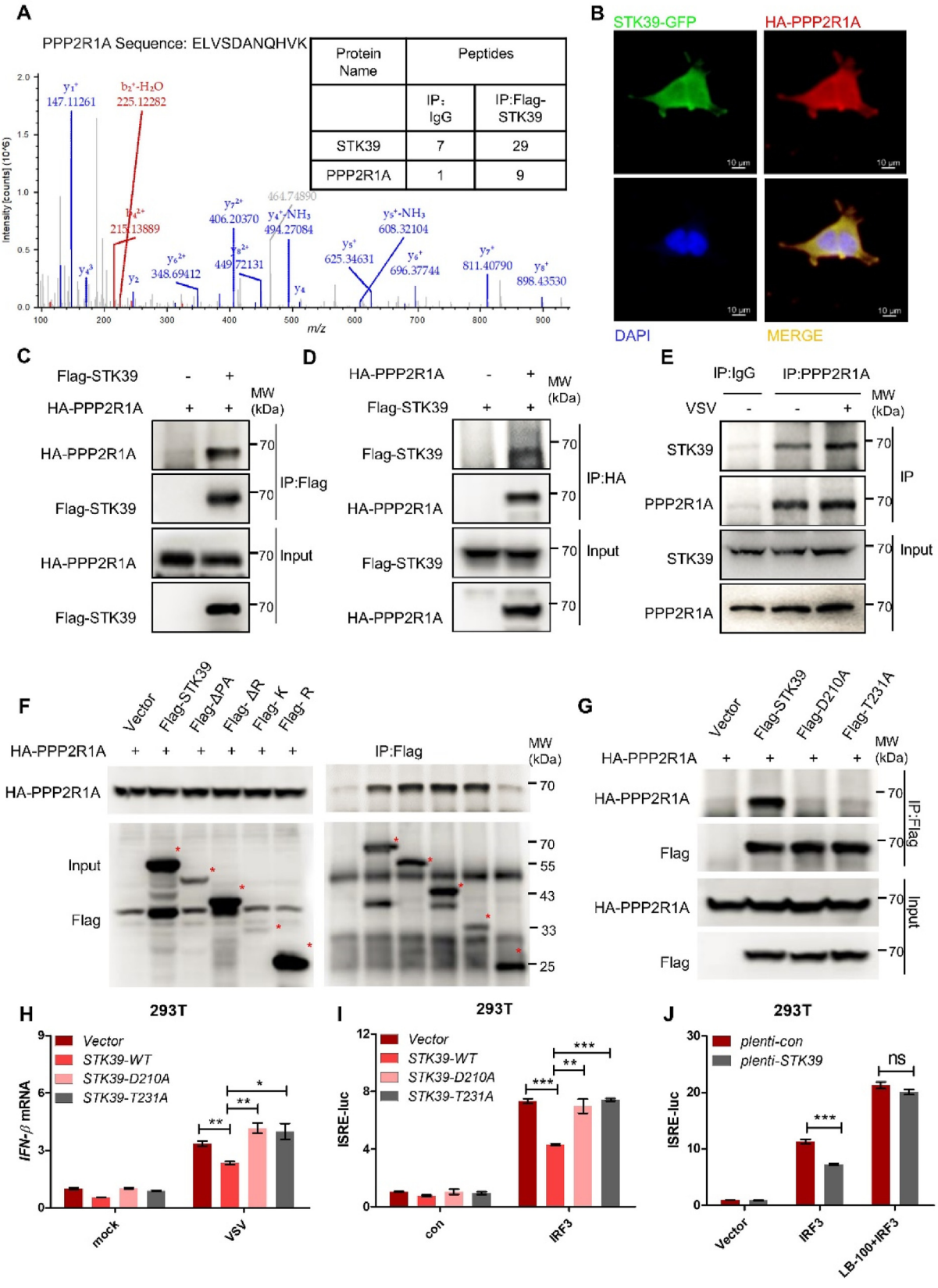

Figure 5 STK39 suppresses the activation of IRF3 by targeting PP2A. (A) Mass spectrometry analysis revealed that STK39 interacts with PPP2R1A. (B) HEK293T cells were co-transfected with STK39-GFP and HA-PPP2R1A plasmids for 72 h. The interaction between STK39 and PPP2R1A was analyzed by confocal microscopy. Scale bar, 10 μm. (C, D) HEK293T cells were co-transfected with Flag-STK39 and HA-PPP2R1A plasmids for 72 h. The interaction between STK39 and PPP2R1A was assessed by immunoprecipitation and immunoblotting. (E)

3.4. STK39 inhibits virus-triggered type I interferon production by inhibiting the phosphorylation of IRF3

TBK1/IRF3, JNK, AKT, and NF-κB signaling pathways are crucial for the regulation of type I interferon production. To determine the molecular mechanisms by which STK39 inhibits the production of type I interferon, control RAW264.7 macrophages and stable Stk39-overexpression RAW264.7 macrophages were infected with VSV and the phosphorylation levels of TBK1/IRF3, JNK, AKT, and NF-κB were analyzed by immunoblotting. As shown in Fig. 4A, overexpression of Stk39 dramatically suppressed VSV-triggered phosphorylation of IRF3, while the phosphorylation levels of JNK, AKT, and NF-κB were little changed. Transfected poly(I:C) to control RAW264.7 macrophages and stable Stk39-overexpression RAW264.7 macrophages also revealed that overexpression of Stk39 decreased the phosphorylation of IRF3 (Fig. 4B). Consistent with these, knockout of *Stk39* in mice macrophages, spleens, and HEK293T cells resulted in a much higher phosphorylation level of IRF3 compared with that in wild-type cells after VSV or poly(I:C) stimulation (Fig. 4C−E and Supporting Information Fig. S5A). These results suggest that STK39 inhibits the phosphorylation of IRF3 during viral infection. To further determine which component involved in STK39 negatively regulates virus-triggered type I interferon expression, IFN-β and ISRE luciferase reporter plasmids were co-transfected with RIG-I, MAVS, TBK1, IRF3, and IRF3-5D (a constitutively active form of IRF3) plasmids to control HEK293T cells and stable STK39-overexpression HEK293T cells, respectively. We found that overexpression of STK39 markedly suppressed RIG-I, MAVS, TBK1, and IRF3-induced IFN-β and ISRE luciferase reporter activity while having little effect on IRF3-5D-induced IFN-β and ISRE luciferase reporter activity (Fig. 4F, G and Fig. S5B). Therefore, these results suggest that STK39 acts on IRF3-mediated type I interferon production.

3.5. STK39 interacts with PPP2R1A

To elucidate how STK39 inhibits the phosphorylation of IRF3, STK39-binding proteins were analyzed by mass spectrometry. We found that PPP2R1A (a scaffold subunit of PP2A) was a partner protein of STK39 (Fig. 5A). As a protein phosphatase, PP2A was reported to promote the dephosphorylation of IRF3 and limit virus-triggered type I interferon production[7]. As a scaffold subunit of PP2A, PPP2R1A is critical for PP2A subunits' stability and PP2A activity[34]. Thus, the interaction between STK39 and PPP2R1A may have contributed to the dephosphorylation of IRF3. To confirm the interaction between STK39 and PPP2R1A, STK39-GFP and HA-PPP2R1A expression plasmids were transfected to HEK293T cells, we found that STK39 and PPP2R1A showed co-localization in HEK293T cells (Fig. 5B). Co-immunoprecipitation assays also indicated that Flag-STK39 interacted with HA-PPP2R1A (Fig. 5C and D). Besides, we found that STK39 also interacted with PPP2R1A in endogenous conditions, and viral infection promoted this process (Fig. 5E). A glutathione S-transferase (GST) pull-down assay showed that STK39 directly interacts with PPP2R1A (Supporting Information Fig. S6A). To validate the specific region of STK39 that binds to PPP2R1A, truncated fragments of STK39 expression plasmids were constructed. Co-immunoprecipitation assays demonstrated that PPP2R1A could not interact with STK39 when the kinase domain of STK39 was deleted. This suggests that the kinase domain of STK39 is required for STK39 to interact with PPP2R1A (Fig. 5F). Thus, we speculated that the kinase activity of STK39 may be involved in the interaction between STK39 and PPP2R1A. Then wild-type and kinase-dead mutations of STK39 (catalytically inactive STK39-D210A and upstream kinase insensitive STK39-T231A) expression plasmids and PPP2R1A expression plasmids were co-transfected into HEK293T cells. Co-immunoprecipitation assays confirmed that the interaction between STK39 and PPP2R1A was abolished by STK39 kinase-dead mutations (Fig. 5G). To evaluate the role of the kinase activity of STK39 in suppressing virus-triggered type I interferon signaling, wild-type and mutant STK39 expression plasmids were transfected into 293T cells and the cells were infected with VSV. As shown in Fig. 5H and Fig. S6B, wild-type STK39 dramatically reduced the expression of VSV-induced IFN-β, while kinase-dead mutations could not. ISRE luciferase reporter assays also showed that the kinase activity of STK39 was responsible for suppressing IRF3-mediated type I interferon expression (Fig. 5I). To confirm whether PP2A was involved in STK39 suppressing virus-triggered type I interferon expression, we next examined the function of PPP2R1A in viral infection. We found that PPP2R1A also negatively regulated virus-triggered type I interferon expression and facilitated viral infection (Fig. S6C−S6E). Most importantly, the inhibitory effect of STK39 on IRF3-induced ISRE luciferase activation and IFN-β expression were blocked by PP2A inhibitors (Fig. 5J and Fig. S6F), overexpression of PPP2R1A in *STK39*-knockout HEK293T cells obviously inhibited the level of *p*-IRF3 and expression of IFN-β induced by *STK39*-knockout but promoted the replication of VSV (Fig. S6G−S6I). Taken together, these data suggest that STK39 interacts with PPP2R1A, and the phosphatase activity of PP2A is essential for STK39 to inhibit virus-triggered type I interferon production.

HEK293T cells were infected with 0.01 MOI VSV for 8 h, and the endogenous association of STK39 and PPP2R1A was assessed by immunoprecipitation and immunoblotting. (F) HEK293T cells were co-transfected with HA-PPP2R1A and Flag-STK39-truncated mutants into 293T cells for 72 h, cell lysates were immunoprecipitated with anti-Flag antibody and the level of HA-PPP2R1A and Flag-STK39-truncated mutants were assessed by immunoblotting. (G) HEK293T cells were co-transfected with HA-PPP2R1A and wild-type or kinase-dead mutations of STK39 plasmids into HEK293T cells for 72 h. Cell lysates were immunoprecipitated with anti-Flag antibody and the levels of HA-PPP2R1A and STK39 were assessed by immunoblotting. (H) Wild-type or kinase-dead mutations of STK39 plasmids were transfected into HEK293T cells, the cells were then infected with VSV for 4 h, and the expression of *IFN-β* was analyzed by qPCR. (I) Wild-type or kinase-dead mutations of STK39 plasmids were co-transfected with ISRE promoter reporter plasmid and *Renilla* reporter plasmid into HEK293T cells for 24 h. The activities of ISRE luciferase were measured with a dual-luciferase reporter assay system. (J) Stable overexpression of STK39 in HEK293T cells, the cells were co-transfected with IRF3 plasmid, ISRE promoter reporter plasmid, and *Renilla* reporter plasmid for 24 h, after being treated with 20 μmol/L PP2A inhibitor LB-100 for 4 h, the activities of ISRE luciferase were measured with a dual-luciferase reporter assay system. Data are shown as mean ± SEM; *$P < 0.05$; **$P < 0.01$; ***$P < 0.001$; ns, not significant.

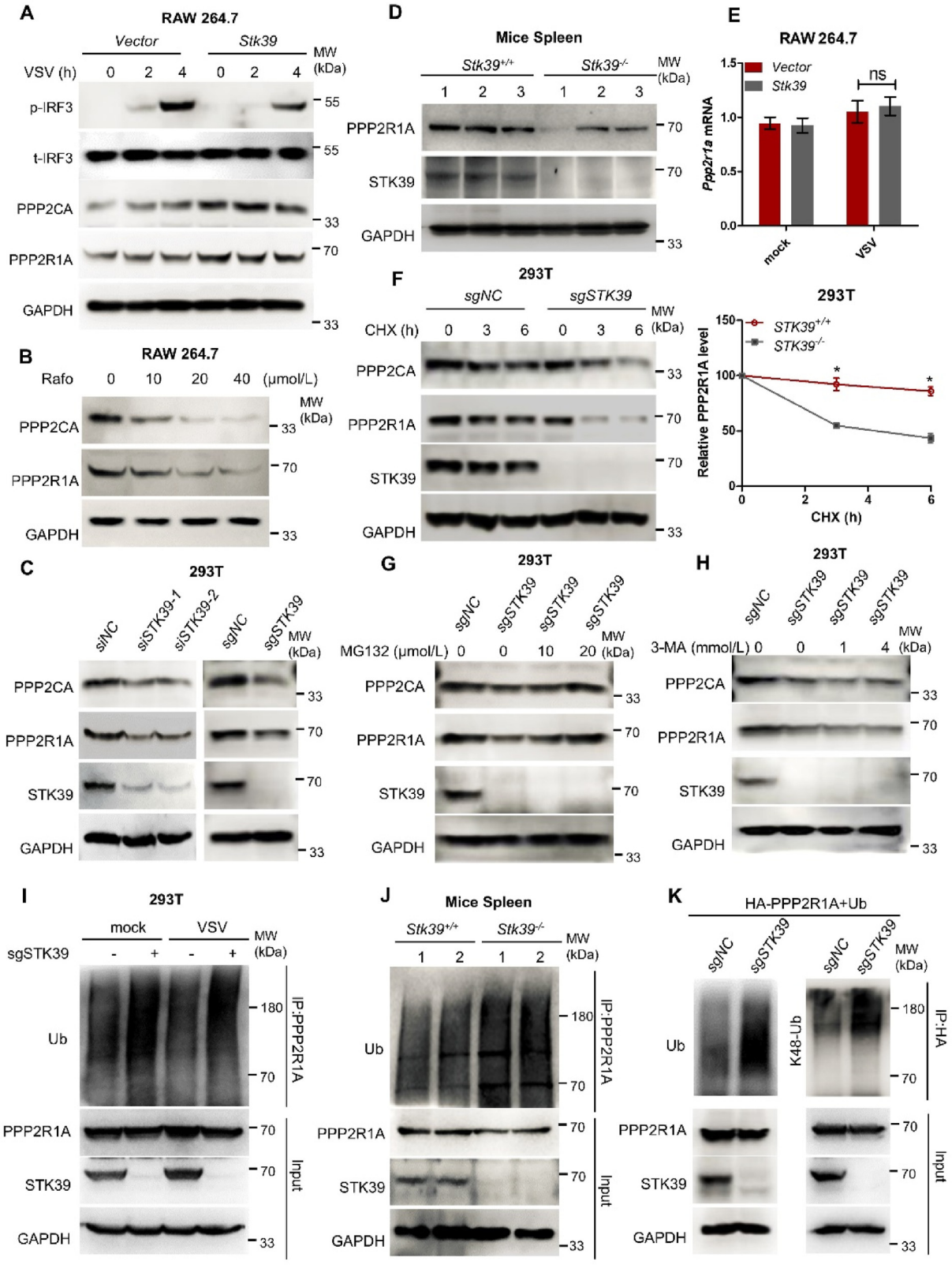

Figure 6 STK39 stabilizes PPP2R1A. (A) Stable overexpression of Stk39 in RAW264.7 cells, the cells were infected with VSV (MOI = 0.1) for the indicated times. Phosphorylated or total IRF3, PPP2CA, and PPP2R1A were assessed by immunoblotting. (B) RAW264.7 cells were treated with indicated concentrations of STK39 inhibitor Rafoxanide for 12 h. The expression of PPP2CA, PPP2R1A, and GAPDH were assessed by immunoblotting. (C) Knockdown or knockout of STK39 in HEK293T cells, the expression of PPP2CA, PPP2R1A, and STK39 were analyzed by immunoblotting. (D) Six-week-old $Stk39^{+/+}$ and $Stk39^{-/-}$ mice were intraperitoneally injected with VSV (5×10^8 pfu/g) for 12 h. The expression of PPP2R1A, STK39, and GAPDH in mice spleens were assessed by immunoblotting. (E) Stable overexpression of Stk39 in

3.6. *STK39 stabilizes PPP2R1A*

Next, we investigated the mechanisms by which STK39 regulates PPP2R1A. Western blotting showed that overexpression of STK39 increased the protein level of PPP2R1A, while inhibition, knockdown, or knockout of *STK39* significantly attenuated the protein level of PPP2R1A *in vitro* and *in vivo* (Fig. 6A−D). However, qPCR showed that STK39 had little influence on the mRNA expression level of *PPP2R1A* (Fig. 6E, Supporting Information Fig. S7A−S7C). Furthermore, the cycloheximide chase assay showed that STK39 maintained the stability of PPP2R1A (Fig. 6F). We then examined whether proteasome or autophagy mediated the stability of PPP2R1A. As shown in Fig. 6G and H, knockout of *STK39* decreased PPP2R1A levels in HEK293T cells and the proteasome inhibitor MG-132 reversed this process, while autophagy inhibitor 3-methyladenine (3-MA) could not, suggesting that STK39 maintained the stability of PPP2R1A *via* the proteasome. Consistent with these results, we found that knockout of *STK39* in HEK293T cells increased the endogenous poly-ubiquitination of PPP2R1A before or after viral infection, and the same phenomenon occurred in *Stk39*-knockout mice spleens (Fig. 6I and J). In addition to these, knockdown or knockout of *STK39* also enhanced the poly-ubiquitination or K48 linked-polyubiquitination (as the K48 linked-polyubiquitination usually promotes proteins to degrade in a manner of proteasome way) of transfected HA-PPP2R1A (Fig. 6K, Fig. S7D). Thus, these data indicate that STK39 stabilizes PPP2R1A by inhibiting PPP2R1A polyubiquitination and proteasome degradation.

3.7. *STK39 stabilizes PP2A by inhibiting DCAF1-mediated PPP2R1A degradation*

A previous study reported that CRL4−DCAF1 ubiquitin E3 ligase induces proteasome degradation of PPP2R1A[22]. Considering that STK39 maintained the stability of PPP2R1A *via* the proteasome, we speculated that DCAF1 may have contributed to the process of STK39 maintaining the stability of PPP2R1A. We first investigated the effect of DCAF1 on antiviral innate immune response. By measuring the expression of VSV-triggered type I interferon, we found that *DCAF1* knockdown significantly decreased the expression of *IFN-α4* and *IFN-β*, while overexpression of DCAF1 increased type I IFN production (Fig. 7A, Supporting Information Fig. S8A and S8B). By testing the VSV RNA level, we found that the DCAF1 knockdown facilitated VSV replication and overexpression of DCAF1 suppressed VSV replication (Fig. 7B). Consistent with these, luciferase reporter assays also showed that DCAF1 positively regulated type I interferon signaling. Overexpression of DCAF1 had little influence on IRF3-5D-induced IFN-*β* and ISRE luciferase activity, and *DCAF1* knockdown decreased VSV-triggered phosphorylation of IRF3 revealed that DCAF1 enhanced antiviral innate immune response by acting on IRF3 (Fig. 7C−E). To validate that DCAF1 induces the degradation of PPP2R1A, immunoblotting and co-immunoprecipitation assays were performed. Results showed that overexpression of DCAF1 decreased the protein level of PPP2R1A, and knockdown of *DCAF1* increased the protein level of PPP2R1A. DCAF1 could interact with PPP2R1A and promote PPP2R1A ubiquitination (Fig. 7F−I, Fig. S8C and S8D). Interestingly, we found that inhibition or knockout of *STK39* enhanced the combination ability of DCAF1 and PPP2R1A, and DCAF1-mediated ubiquitination of PPP2R1A, while overexpression of STK39 suppressed these processes, knockdown of *DCAF1* in *STK39*-knockout HEK293T cells could rescue the degradation of PPP2R1A and inhibit the upregulation of *IFN-β* and *ISG15* induced by *STK39*-knockout (Fig. 7F−J, Fig. S8E−S8H). Collectively, our results reveal that STK39 suppresses the phosphorylation of IRF3 by inhibiting DCAF1-mediated PPP2R1A degradation.

4. Discussion

Previous studies showed that STK39 is involved in various biological processes, especially ion homeostasis and tumor progression[27,33,35]. However, very little is known about its role in antiviral immune response. In the current study, we found that viral infection (including RNA and DNA virus) significantly induced STK39 expression. Pharmacological inhibition of virus-related signaling pathways revealed that NF-κB, SP1, and STAT1 were crucial for viral infection-induced expression of STK39, which suggests that viral infection upregulates STK39 through multiple signaling pathways. Next, our studies demonstrated that overexpressed STK39 negatively regulated type I interferon signaling and promoted viral replication. This indicates that STK39 is crucial for viral immune escape. STK39 inhibitors dramatically suppressed viral replication, demonstrating that STK39 could be a potential therapeutic target for viral infectious diseases. Further experiments showed that PPP2R1A, a scaffold subunit of the PP2A complex, is involved in STK39-mediated type I interferon signal suppression, suggesting that PP2A is critical for STK39-mediated viral immune escape.

PP2A participates in the development of multitudinous diseases, such as autoimmune diseases[36], inflammatory diseases[37], viral infectious diseases, and tumorigenesis[38,39]. Most studies of PP2A were focused on its catalytic subunit, which directly dephosphorylates target proteins to regulate a variety of biological functions. Still, relatively little research has been done on the

RAW264.7 cells, the cells were infected with VSV for 4 h. The expression of *Ppp2r1a* was analyzed by qPCR. (F) Wild-type and *STK39*-knockout HEK293T cells were treated with 1 μmol/L CHX for the indicated time. The expression of PPP2CA, PPP2R1A, and STK39 were analyzed by immunoblotting. (G) *STK39*-knockout HEK293T cells were treated with indicated concentrations of MG132 for 8 h. The expression of PPP2CA, PPP2R1A, and STK39 were analyzed by immunoblotting. (H) *STK39*-knockout HEK293T cells were treated with indicated concentrations of 3-MA for 8 h. The expression of PPP2CA, PPP2R1A, and STK39 were analyzed by immunoblotting. (I) Wild-type and *STK39*-knockout HEK293T cells were infected with VSV (MOI = 0.01) for 6 h. The endogenous ubiquitination of PPP2R1A was analyzed by immunoprecipitation and immunoblotting. (J) Six-week-old $Stk39^{+/+}$ and $Stk39^{-/-}$ mice were intraperitoneally injected with VSV (5×10^8 pfu/g) for 12 h. The endogenous ubiquitination of PPP2R1A in mice spleens was assessed by immunoprecipitation and immunoblotting. (K) Wild-type and *STK39*-knockout HEK293T cells were co-transfected with HA-PPP2R1A and ubiquitin plasmids for 72 h. The ubiquitination and K48 linked-polyubiquitination of HA-PPP2R1A were analyzed by immunoprecipitation and immunoblotting. Data are shown as mean ± SEM; $^*P < 0.05$; ns, not significant.

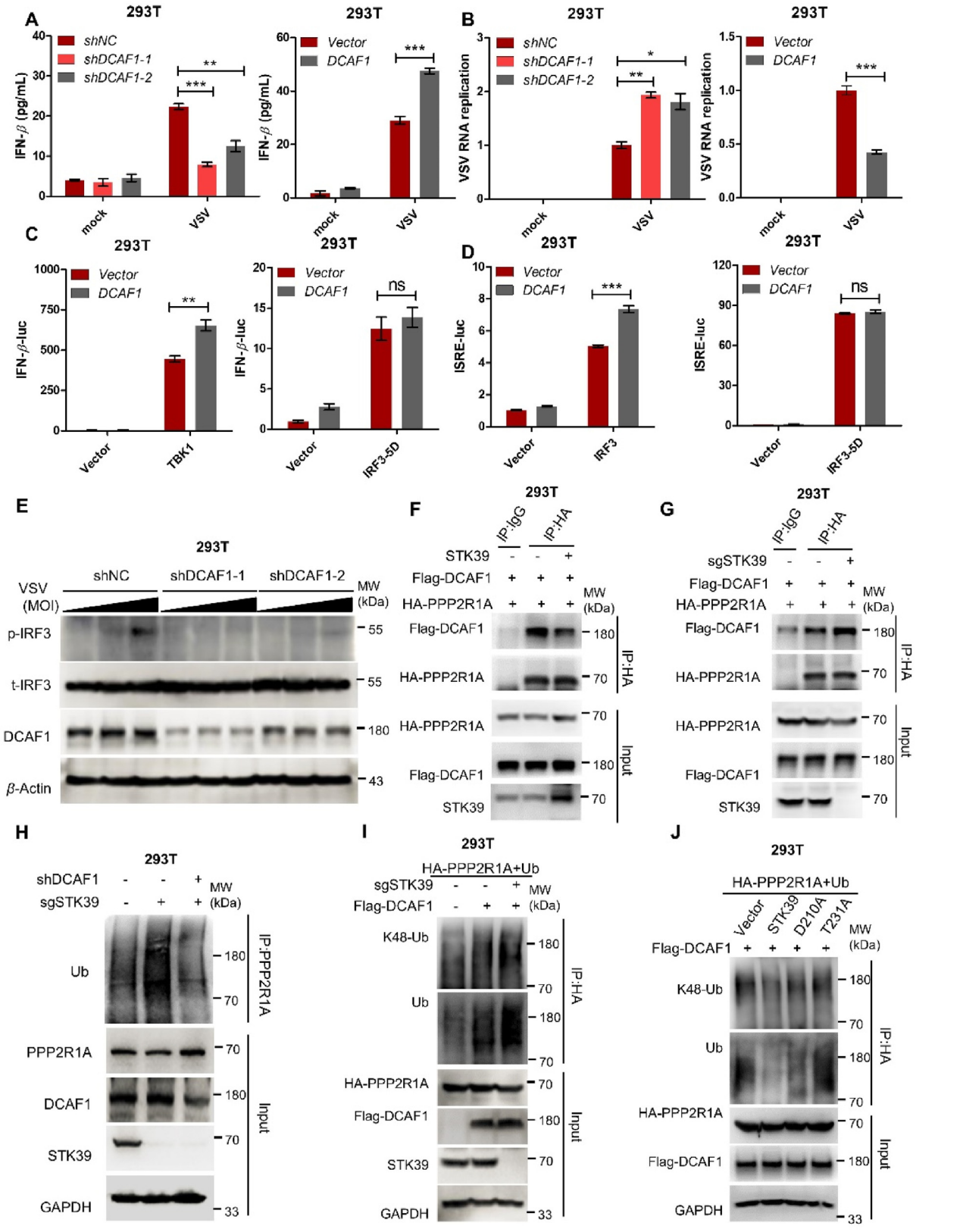

Figure 7 STK39 inhibits DCAF1-mediated PPP2R1A degradation. (A) Knockdown or overexpression of DCAF1 in HEK293T cells. The cells were infected with VSV for 12 h. The production of IFN-β was measured by ELISA. (B) Knockdown or overexpression of DCAF1 in HEK293T cells. The cells were infected with VSV for 12 h. VSV RNA replicates were detected by qPCR. (C) HEK293T cells were co-transfected with DCAF1 plasmid, IFN-β promoter reporter plasmid, *Renilla* reporter plasmid, and the indicated protein plasmid for 24 h. The activities of IFN-β luciferase were measured with a dual-luciferase reporter assay system. (D) HEK293T cells were co-transfected with DCAF1 plasmid, ISRE

scaffold subunit. Accumulating evidence has shown that the scaffold subunit of PP2A also contributes to the catalytic activity of PP2A and is critical for various biological functions[40,41]. In this study, to elucidate the underlying mechanisms by which STK39 inhibits IRF3-mediated type I interferon pathway, STK39-binding proteins were analyzed by mass spectrometry. We found that the scaffold subunit of PP2A (PPP2R1A) could bind to STK39. Subsequent experiments showed that STK39 regulated the activity of PP2A by maintaining the stability of PPP2R1A. Blocking the activity of PP2A eliminated STK39-mediated suppression of interferon signaling, suggesting that STK39 inhibits IRF3-mediated type I interferon is dependent on PP2A. A confusing question raised here is that the kinase-dead mutants of STK39 did not interact with PPP2R1A in HEK293T cells. However, GST-STK39, which was not phosphorylated on the T231 site, still exhibited interaction with His-PPP2R1A. For this question, we speculated that maybe other molecules or mechanisms were involved in the interaction of STK39 and PPP2R1A in mammalian cells. Thus, the detailed interaction mechanism between STK39 and PPP2R1A still needs further study.

$CRL4^{DCAF1}$-mediated degradation of PPP2R1A is crucial for regulating oocyte meiosis and an important way to control the activity of PP2A[22]. To investigate how STK39 maintains the stability of PPP2R1A, we tested the influence of STK39 on the process $CRL4^{DCAF1}$-mediated degradation of PPP2R1A. Experimental results showed that overexpression of STK39 reduced the combination ability of DCAF1 and PPP2R1A and DCAF1-mediated ubiquitination of PPP2R1A, implying that DCAF1-mediated PPP2R1A degradation contributed to the process of STK39-mediated viral immune escape. By knocking down or overexpressing DCAF1 in HEK293T cells, we discovered that DCAF1 was a positive regulator of type I interferon signaling by facilitating proteasome degradation of PP2A.

As a serine/threonine kinase, STK39 usually exerts its biological functions by regulating the phosphorylation of downstream proteins. This study found that catalytically inactive STK39 would not restrain antiviral immune response, indicating that STK39 negatively regulates type I interferon signaling in a kinase activity-dependent manner. In addition, we found that STK39 inhibited DCAF1-mediated degradation of PP2A, which was also dependent on its protein kinase activity, suggesting that the kinase activity of STK39 also implicates in the process of DCAF1-mediated degradation of PP2A. However, whether STK39 can directly regulate the phosphorylation of PP2A still needs to be explored in the future.

5. Conclusions

In summary, we demonstrated that STK39 acts as a new negative regulator of antiviral type I interferon signaling by restraining DCAF1-mediated proteasome degradation of PP2A. We also showed that the component of CRL4−DCAF1 ubiquitin E3 ligase (DCAF1) promoted antiviral immunity. Pharmacological inhibition of STK39 markedly ameliorated viral infection-induced lung injury and viral replication, suggesting that STK39 could be a potential therapeutic target for viral infectious diseases.

Acknowledgements

This work was supported by the National Natural Science Foundation of China (No. 82101849 to Chengfei Zhang, 82072739 to Hongping Xia, 82273162 to Guoren Zhou), The Recruitment Program of Overseas High-Level Young Talents, and starting up funding of Southeast University(4024002312, China), Jiangsu Cancer Hospital Spark Fundamental Research Special Fund (ZJ202103, China), Jiangsu Province Health Care and Elderly Health Research Key Topics (LKZ2022007, China), Nanjing Health Science and Technology Development Special Project (YKK22204 to Chengfei Zhang, YKK23204 to Xin Chen, China).

Author contributions

Chengfei Zhang: Conceptualization (lead); Investigation (equal); Methodology (lead); Writing − original draft (lead); Formal analysis (lead). Ping Xu: Investigation (equal); Methodology (equal). Yongsheng Wang: Resources; Funding acquisition. Xin Chen: Investigation (equal); Methodology (equal). Yue Pan, Zhijie Ma, Cheng Wang, Haojun Xu : Conceptualization (supporting); Investigation and Methodology (supporting); Guoren Zhou, Feng Zhu: Resources, Funding acquisition, Conceptualization. Hongping Xia: Writing − review & editing, Supervision, Resources, Funding acquisition, Conceptualization.

Conflicts of interest

The authors have declared that they have no conflicts of interest.

Appendix A. Supporting information

Supporting information to this article can be found online at https://doi.org/10.1016/j.apsb.2024.12.034.

promoter reporter plasmid, *Renilla* reporter plasmid, and the indicated protein plasmid for 24 h. The activities of ISRE luciferase were measured with a dual-luciferase reporter assay system. (E) Knockdown of *DCAF1* in HEK293T cells. The cells were infected with VSV (0.01, 0.03 MOI) for 4 h. Phosphorylated or total IRF3 and DCAF1 were assessed by immunoblotting. (F) Overexpression of STK39 in HEK293T cells. The cells were co-transfected with Flag-DCAF1 and HA-PPP2R1A plasmids for 72 h. The interaction between DCAF1 and PPP2R1A was assessed by immunoprecipitation and immunoblotting. (G) Wild-type and *STK39*-knockout HEK293T cells were co-transfected with Flag-DCAF1 and HA-PPP2R1A plasmids for 72 h. The interaction between DCAF1 and PPP2R1A was assessed by immunoprecipitation and immunoblotting. (H) Knockdown of *DCAF1* in *STK39*-knockout HEK293T cells. The expression of PPP2R1A, DCAF1, and STK39 were analyzed by immunoblotting, and the endogenous ubiquitination of PPP2R1A was analyzed by immunoprecipitation and immunoblotting. (I) Wild-type and *STK39*-knockout HEK293T cells were co-transfected with Flag-DCAF1, HA-PPP2R1A, and ubiquitin plasmids for 72 h. The ubiquitination and K48 linked-polyubiquitination of HA-PPP2R1A were assessed by immunoprecipitation and immunoblotting. (J) Overexpression of Wild-type or kinase-dead mutations of STK39 in HEK293T cells. The cells were co-transfected with Flag-DCAF1, HA-PPP2R1A, and ubiquitin plasmids for 72 h. The ubiquitination and K48 linked-polyubiquitination of HA-PPP2R1A were assessed by immunoprecipitation and immunoblotting. Data are shown as mean ± SEM; $^{*}P < 0.05$; $^{**}P < 0.01$; $^{***}P < 0.001$; ns, not significant.

References

1. Liu SY, Aliyari R, Chikere K, Li G, Marsden MD, Smith JK, et al. Interferon-inducible cholesterol-25-hydroxylase broadly inhibits viral entry by production of 25-hydroxycholesterol. *Immunity* 2013;**38**:92−105.
2. Hu Z, Xie Y, Lu J, Yang J, Zhang J, Jiang H, et al. VANGL2 inhibits antiviral IFN-I signaling by targeting TBK1 for autophagic degradation. *Sci Adv* 2023;**9**:eadg2339.
3. Yi D, An N, Li Q, Liu Q, Shao H, Zhou R, et al. Interferon-induced MXB protein restricts vimentin-dependent viral infection. *Acta Pharm Sin B* 2024;**14**:2520−36.
4. Chen W, Han C, Xie B, Hu X, Yu Q, Shi L, et al. Induction of Siglec-G by RNA viruses inhibits the innate immune response by promoting RIG-I degradation. *Cell* 2013;**152**:467−78.
5. Kang NX, Zou Y, Liang QH, Wang YE, Liu YL, Xu GQ, et al. Anemoside B4 inhibits enterovirus 71 propagation in mice through upregulating 14-3-3 expression and type I interferon responses. *Acta Pharmacol Sin* 2022;**43**:977−91.
6. Wu J, Chen ZJ. Innate immune sensing and signaling of cytosolic nucleic acids. *Annu Rev Immunol* 2014;**32**:461−88.
7. Long L, Deng Y, Yao F, Guan D, Feng Y, Jiang H, et al. Recruitment of phosphatase PP2A by RACK1 adaptor protein deactivates transcription factor IRF3 and limits type I interferon signaling. *Immunity* 2014;**40**:515−29.
8. Liang X, Liu K, Jia X, Cheng C, Zhang M, Kong L, et al. Suppressing FXR promotes antiviral effects of bile acids *via* enhancing the interferon transcription. *Acta Pharm Sin B* 2024;**14**:3513−27.
9. Glon D, Vilmen G, Perdiz D, Hernandez E, Beauclair G, Quignon F, et al. Essential role of hyperacetylated microtubules in innate immunity escape orchestrated by the EBV-encoded BHRF1 protein. *PLoS Pathog* 2022;**18**:e1010371.
10. García-Sastre A, Biron CA. Type 1 interferons and the virus−host relationship: a lesson in détente. *Science* 2006;**312**:879−82.
11. Cortez V, Livingston B, Sharp B, Hargest V, Papizan JB, Pedicino N, et al. Indoleamine 2,3-dioxygenase 1 regulates cell permissivity to astrovirus infection. *Mucosal Immunol* 2023;**16**:551−62.
12. Nitta S, Sakamoto N, Nakagawa M, Kakinuma S, Mishima K, Kusano-Kitazume A, et al. Hepatitis C virus NS4B protein targets STING and abrogates RIG-I-mediated type I interferon-dependent innate immunity. *Hepatology* 2013;**57**:46−58.
13. Choi HJ, Park A, Kang S, Lee E, Lee TA, Ra EA, et al. Human cytomegalovirus-encoded US9 targets MAVS and STING signaling to evade type I interferon immune responses. *Nat Commun* 2018;**9**:125.
14. Shi Y. Serine/threonine phosphatases: mechanism through structure. *Cell* 2009;**139**:468−84.
15. Vit G, Duro J, Rajendraprasad G, Hertz EPT, Holland LKK, Weisser MB, et al. Chemogenetic profiling reveals PP2A-independent cytotoxicity of proposed PP2A activators iHAP1 and DT-061. *EMBO J* 2022;**41**:e110611.
16. Taylor SE, O'Connor CM, Wang Z, Shen G, Song H, Leonard D, et al. The highly recurrent PP2A Aα-subunit mutation P179R alters protein structure and impairs PP2A enzyme function to promote endometrial tumorigenesis. *Cancer Res* 2019;**79**:4242−57.
17. Bian Y, Kitagawa R, Bansal PK, Fujii Y, Stepanov A, Kitagawa K. Synthetic genetic array screen identifies PP2A as a therapeutic target in Mad2-overexpressing tumors. *Proc Natl Acad Sci U S A* 2014;**111**:1628−33.
18. Zhang S, Feng Y, Narayan O, Zhao LJ. Cytoplasmic retention of HIV-1 regulatory protein Vpr by protein−protein interaction with a novel human cytoplasmic protein VprBP. *Gene* 2001;**263**:131−40.
19. Ghate NB, Kim S, Mehmood R, Shin Y, Kim K, An W. VprBP/DCAF1 regulates p53 function and stability through site-specific phosphorylation. *Oncogene* 2023;**42**:1405−16.
20. Han XR, Sasaki N, Jackson SC, Wang P, Li Z, Smith MD, et al. CRL4(DCAF1/VprBP) E3 ubiquitin ligase controls ribosome biogenesis, cell proliferation, and development. *Sci Adv* 2020;**6**:eabd6078.
21. Ghate NB, Kim S, Shin Y, Kim J, Doche M, Valena S, et al. Phosphorylation and stabilization of EZH2 by DCAF1/VprBP trigger aberrant gene silencing in colon cancer. *Nat Commun* 2023;**14**:2140.
22. Yu C, Ji SY, Sha QQ, Sun QY, Fan HY. CRL4-DCAF1 ubiquitin E3 ligase directs protein phosphatase 2A degradation to control oocyte meiotic maturation. *Nat Commun* 2015;**6**:8017.
23. Tsutsumi T, Ushiro H, Kosaka T, Kayahara T, Nakano K. Proline- and alanine-rich Ste20-related kinase associates with F-actin and translocates from the cytosol to cytoskeleton upon cellular stresses. *J Biol Chem* 2000;**275**:9157−62.
24. Qiu Z, Dong B, Guo W, Piotr R, Longmore G, Yang X, et al. STK39 promotes breast cancer invasion and metastasis by increasing SNAI1 activity upon phosphorylation. *Theranostics* 2021;**11**:7658−70.
25. Taylor CAt, An SW, Kankanamalage SG, Stippec S, Earnest S, Trivedi AT, et al. OSR1 regulates a subset of inward rectifier potassium channels *via* a binding motif variant. *Proc Natl Acad Sci U S A* 2018;**115**:3840−5.
26. McCormick JA, Mutig K, Nelson JH, Saritas T, Hoorn EJ, Yang CL, et al. A SPAK isoform switch modulates renal salt transport and blood pressure. *Cell Metab* 2011;**14**:352−64.
27. Hao X, Zhang Y, Lu Y, Han G, Rong D, Sun G, et al. STK39 enhances the progression of Cholangiocarcinoma *via* PI3K/AKT pathway. *iScience* 2021;**24**:103223.
28. Zhang C, Wang X, Fang D, Xu P, Mo X, Hu C, et al. STK39 is a novel kinase contributing to the progression of hepatocellular carcinoma by the PLK1/ERK signaling pathway. *Theranostics* 2021;**11**:2108−22.
29. Zhang C, He H, Wang L, Zhang N, Huang H, Xiong Q, et al. Virus-triggered ATP release limits viral replication through facilitating IFN-β production in a P2X7-dependent manner. *J Immunol* 2017;**199**:1372−81.
30. Zhang C, Yan Y, He H, Wang L, Zhang N, Zhang J, et al. IFN-stimulated P2Y13 protects mice from viral infection by suppressing the cAMP/EPAC1 signaling pathway. *J Mol Cell Biol* 2019;**11**:395−407.
31. Huang H, Xiong Q, Wang N, Chen R, Ren H, Siwko S, et al. Kisspeptin/GPR54 signaling restricts antiviral innate immune response through regulating calcineurin phosphatase activity. *Sci Adv* 2018;**4**:eaas9784.
32. Zhang C, Qin J, Zhang S, Zhang N, Tan B, Siwko S, et al. ADP/$P2Y_1$ aggravates inflammatory bowel disease through ERK5-mediated NLRP3 inflammasome activation. *Mucosal Immunol* 2020;**13**:931−45.
33. Zhang J, Bhuiyan MIH, Zhang T, Karimy JK, Wu Z, Fiesler VM, et al. Modulation of brain cation−Cl^- cotransport *via* the SPAK kinase inhibitor ZT-1a. *Nat Commun* 2020;**11**:78.
34. Chi RA, Wang T, Huang CL, Wu SP, Young SL, Lydon JP, et al. WNK1 regulates uterine homeostasis and its ability to support pregnancy. *JCI insight* 2020;**5**:e141832.
35. Vachel L, Shcheynikov N, Yamazaki O, Fremder M, Ohana E, Son A, et al. Modulation of Cl^- signaling and ion transport by recruitment of kinases and phosphatases mediated by the regulatory protein IRBIT. *Sci Signal* 2018;**11**:eaat5018.
36. Jiang Y, Jin X, Chi Z, Bai Y, Manthiram K, Mudd P, et al. Protein phosphatase 2A propels follicular T helper cell development in lupus. *J Autoimmun* 2023;**136**:103028.
37. Wu Y, Hu Y, Wang B, Li S, Ma C, Liu X, et al. Dopamine uses the DRD5−ARRB2−PP2A signaling axis to block the TRAF6-mediated NF-κB pathway and suppress systemic inflammation. *Mol Cell* 2020;**78**:42−56.e6.
38. Zuo Q, Liao L, Yao ZT, Liu YP, Wang DK, Li SJ, et al. Targeting PP2A with lomitapide suppresses colorectal tumorigenesis through the activation of AMPK/Beclin1-mediated autophagy. *Cancer Lett* 2021;**521**:281−93.
39. Xi J, Luckenbaugh L, Hu J. Multiple roles of PP2A binding motif in hepatitis B virus core linker and PP2A in regulating core

phosphorylation state and viral replication. *PLoS Pathog* 2021;**17**: e1009230.

40. O'Connor CM, Leonard D, Wiredja D, Avelar RA, Wang Z, Schlatzer D, et al. Inactivation of PP2A by a recurrent mutation drives resistance to MEK inhibitors. *Oncogene* 2020;**39**:703−17.

41. Lenaerts L, Reynhout S, Verbinnen I, Laumonnier F, Toutain A, Bonnet-Brilhault F, et al. The broad phenotypic spectrum of PPP2R1A-related neurodevelopmental disorders correlates with the degree of biochemical dysfunction. *Genet Med* 2021;**23**: 352−62.